Nanoscale Research Letters
a SpringerOpen Journal

NANO EXPRESS Open Access

Hydrothermal synthesis of MnO_2/CNT nanocomposite with a CNT core/porous MnO_2 sheath hierarchy architecture for supercapacitors

Hui Xia[1*], Yu Wang[2], Jianyi Lin[2] and Li Lu[3*]

Abstract

MnO_2/carbon nanotube [CNT] nanocomposites with a CNT core/porous MnO_2 sheath hierarchy architecture are synthesized by a simple hydrothermal treatment. X-ray diffraction and Raman spectroscopy analyses reveal that birnessite-type MnO_2 is produced through the hydrothermal synthesis. Morphological characterization reveals that three-dimensional hierarchy architecture is built with a highly porous layer consisting of interconnected MnO_2 nanoflakes uniformly coated on the CNT surface. The nanocomposite with a composition of 72 wt.% ($K_{0.2}MnO_2{\cdot}0.33H_2O$)/28 wt.% CNT has a large specific surface area of 237.8 m^2/g. Electrochemical properties of the CNT, the pure MnO_2, and the MnO_2/CNT nanocomposite electrodes are investigated by cyclic voltammetry and electrochemical impedance spectroscopy measurements. The MnO_2/CNT nanocomposite electrode exhibits much larger specific capacitance compared with both the CNT electrode and the pure MnO_2 electrode and significantly improves rate capability compared to the pure MnO_2 electrode. The superior supercapacitive performance of the MnO_2/CNT nancomposite electrode is due to its high specific surface area and unique hierarchy architecture which facilitate fast electron and ion transport.

Introduction

In recent years, manganese oxides have attracted considerable research interest due to their distinctive physical and chemical properties and wide applications in catalysis, ion exchange, molecular adsorption, biosensor, and energy storage [1-8]. Specifically, manganese dioxide [MnO_2] has been considered as a promising electrode material for supercapacitors because of its low cost, environmental benignity, and excellent capacitive performance in aqueous electrolytes [9-15]. In aqueous electrolytes, the charging mechanism of MnO_2 may be described by the following reaction [10]:

$$MnO_2 + M^+ + e^- \Leftrightarrow MnOOM, \quad (1)$$

where M represents protons (H^+) and/or alkali cations such as K^+, Na^+, and Li^+. The charge storage is based either on the adsorption of cations at the surface of the electrode material or on the intercalation of cations in the bulk of the electrode material. In order to achieve high capacitive performance, a large surface area and a fast ion/electron transport of the electrode material are required. Therefore, extensive research has been focused on the synthesis of nanostructured MnO_2 as the nanoscale powder, which provides not only a high specific surface area, but also a fast ion and electron transport [16-25]. Various forms of MnO_2 including one-dimensional (nanorods, nanowires, nanobelts, nanotubes) [16-22], two-dimensional [2-D] (nanosheets, nanoflakes) [23-25], and three-dimensional [3-D] (nanospheres, nanoflowers) [26-28] nanostructures have been synthesized. However, the reported specific capacitance values for the various nanostructured MnO_2 electrodes are still far below the theoretical value (approximately 1,370 F/g) [29], which may be attributed to the intrinsically poor electronic conductivity of MnO_2. To improve the capacitive performance of MnO_2, the key is to add conductive additives to improve the electron transport [30]. Due to their excellent electrical conductivity and high specific surface area, carbon nanotubes [CNTs] are now intensively used with MnO_2 to make nanocomposites.

* Correspondence: jasonxiahui@gmail.com; mpeluli@nus.edu.sg
[1]School of Materials Science and Engineering, Nanjing University of Science and Technology, 200 Xiao Ling Wei, Nanjing, 210094, China
[3]Department of Mechanical Engineering, National University of Singapore, 9 Engineering Drive 1, 117576, Singapore
Full list of author information is available at the end of the article

Recently, MnO_2/CNT nanocomposites have been prepared by various methods to improve the electrochemical utilization of MnO_2 and electronic conductivity of the electrode [31-38]. In most studies, once the coated MnO_2 layer becomes thick, it exhibits a dense structure, which is not beneficial for maximizing the utilization of MnO_2 as only the surface area is involved in charge storage. However, if the coated MnO_2 layer is too thin, the specific capacitance of the composite is difficult to be increased as the MnO_2 loading becomes too low. In previous reports, although the MnO_2 incorporation improves the capacitance of the CNT assembly, the overall specific capacitance remains typically less than 200 F/g. In order to increase the MnO_2 loading in the composite while retaining the formation of a nanoscopic MnO_2 phase, depositing a highly porous MnO_2 layer on the CNTs could be a strategy to achieve this goal. However, a facile and fast synthesis of a uniformly distributed MnO_2 porous layer on the CNTs is still a challenge. It could be a beneficial design if one of the nanostructures (nanowire, nanorod, nanoflake, etc.) of MnO_2 could be transferred onto the CNTs as this hierarchy architecture may be able to provide a large specific surface area (due to the porous feature of the MnO_2 sheath) and a fast electron and ion transport (due to the support of the CNT core and the formation of the nanoscopic MnO_2 phase).

In the present work, a facile hydrothermal synthesis has been designed to deposit a uniform and highly porous MnO_2 layer consisting of interconnected nanoflakes onto the surface of the CNTs. The structure, surface morphology, composition, and specific surface area of the as-prepared nanoflaky MnO_2/CNT nanocomposites have been fully investigated. The capacitive behaviors of the CNTs, the pure MnO_2, and the MnO_2/CNT nanocomposite electrodes were also investigated and compared. The advantages of the present MnO_2/CNT hierarchy architecture associated with its superior capacitive behaviors were discussed.

Experimental section

Commercial multiwalled CNTs (20 to 50 nm in diameter, Shenzhen Nanotech Port Co., Ltd., Shenzhen, China) were purified by refluxing the as-received sample in 10 wt.% nitric acid for 12 h. The acid-treated CNTs were then collected by filtration and dried at 120°C for 12 h in vacuum. A typical synthesis process of the MnO_2/CNT nanocomposite is described as follows. Firstly, 0.1 g CNTs was dispersed in 25 ml deionized [DI] water by ultrasonic vibration for 2 h. Then, 0.3 g $KMnO_4$ was added into the above suspension, and the mixed solution was stirred by a magnetic bar for 2 h. After that, the mixed solution was transferred to a 30-mL, Teflon-lined, stainless steel autoclave. The autoclave was sealed and put in an electric oven at 150°C for 6 h and then naturally cooled to room temperature. After the hydrothermal treatment, the resultant samples were collected by filtration and washed with DI water. MnO_2/CNT nanocomposites were finally dried in an oven at 100°C for 12 h for further characterization. To prepare the MnO_2 powders, 0.3 g $KMnO_4$ and 0.2 mL H_2SO_4 (95 wt.%) were placed into 25 mL DI water to form the precursor. The precursor solution was then treated with a hydrothermal reaction in a 30-mL autoclave at 150°C for 4 h.

The crystallographic information of the products was investigated by X-ray diffraction [XRD] (Shimadzu X-ray diffractometer 6000, Cu Kα radiation, Kyoto, Japan) with a scan rate of 2°/min. Morphologies of the acid-treated CNTs, the MnO_2 powders, and the MnO_2/CNT nanocomposites were characterized by field emission scanning electron microscopy [FESEM] (Hitachi S4300, Tokyo, Japan). The morphology and structure of the MnO_2/CNT nanocomposites were further investigated by transmission electron microscopy [TEM] and high-resolution transmission electron microscopy [HRTEM] (JEM-2010, JEOL, Tokyo, Japan). Compositional investigation of the samples was carried out with energy-dispersive X-ray [EDX] spectroscopy (Noran System SIX, Thermo Fisher Scientific, Shanghai, China). The contents of the interlayer water and CNTs of the nanocomposites were determined by thermogravimetric analysis [TGA] (Shimadzu DTG-60H, Kyoto, Japan). Nitrogen adsorption and desorption isotherms at 77.3 K were obtained with a Quantachrome Autosorb-6B (Beijing, China) surface area and a pore size analyzer.

Electrochemical measurements were carried out on three-electrode cells using a Solartron 1287 electrochemical interface combined with a Solartron 1260 frequency response analyzer (Hampshire, United Kingdom). To prepare the working electrode, 80 wt.% of the active material (CNTs, pure MnO_2 powder, or MnO_2/CNT nanocomposite), 15 wt.% carbon black, and 5 wt.% polyvinylidene difluoride dissolved in *N*-methylpyrrolidone were mixed to form a slurry. The slurry was pasted onto a Ti foil and dried for 12 h in a vacuum oven. The loading of the working electrode is typically in the range of 2 to 3 mg/cm^2. A carbon rod was used as the counter electrode, an Ag/AgCl (saturated KCl) electrode was used as the reference electrode, and a 1-M Na_2SO_4 solution was used as the electrolyte. Cyclic voltammetry [CV] and electrochemical impedance spectroscopy [EIS] were utilized to evaluate the electrochemical behaviors of the different composite electrodes. CV measurements were carried out between 0 and 0.9 V (vs. Ag/AgCl) at different scan rates ranging from 10 to 100 mV/s. EIS measurements were carried out in a frequency range from 10 kHz to 0.01 Hz with an ac amplitude of 10 mV.

Results and discussion

XRD patterns of the CNTs, the pure MnO_2 powder, and the MnO_2/CNT nanocomposite are shown in Figure 1. The XRD pattern of the CNTs shows three diffraction peaks at 26.5°, 43.2° and 54.2° which can be indexed as the (002), (100), and (004) reflections of graphite, respectively [39]. The XRD pattern of the pure MnO_2 powder synthesized by hydrothermal reaction can be indexed to the monoclinic potassium birnessite (JCPDS number 80-1098), which consists of 2-D, edge-shared MnO_6 octahedral layers with K^+ cations and water molecules in the interlayer space. The two stronger diffraction peaks correspond to (001) and (002) basal reflections, while another two weaker diffraction peaks can be indexed as the (20*l*/11*l*) and (02*l*/31*l*) diffraction bands, respectively [24]. From the XRD pattern of the MnO_2/CNT nanocomposite, diffraction peaks from the birnessite-type MnO_2 phase can be observed while the diffraction peaks from the CNTs are not obvious due to the coating of the MnO_2 layer.

The structural features of the MnO_2/CNT nanocomposite were further investigated using Raman measurements as shown in Figure 2. Three Raman bands at 1,577 (G band), 1,327 (D band), and 2,652 cm^{-1} (2D band) are observed in Figure 2a for the pristine CNTs, which originate from the Raman-active, in-plane atomic displacement E2g mode, disorder-induced features of the CNTs and the overtone of D band [36]. As shown in Figure 2b, three Raman bands located at 501, 575, and 645 cm^{-1} for the MnO_2 powder are in good agreement with the three major vibrational features of the birnessite-type MnO_2 compounds previously reported at 500 to 510, 575 to 585, and 625 to 650 cm^{-1} [40]. Three Raman bands for the birnessite-type MnO_2 and three

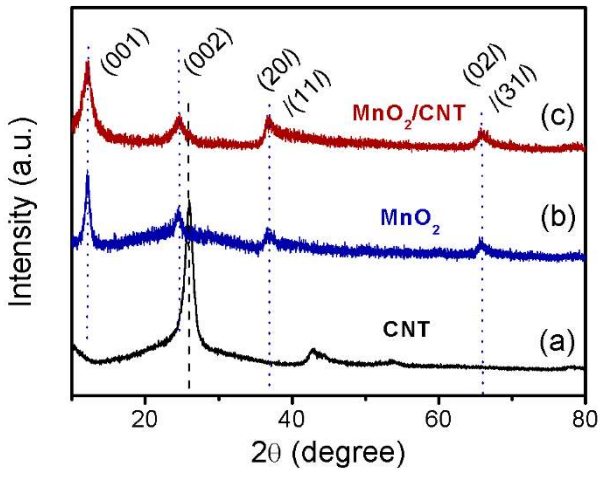

Figure 1 XRD patterns of the (a) pristine CNTs, (b) pure MnO_2, and (c) MnO_2/CNT nanocomposite.

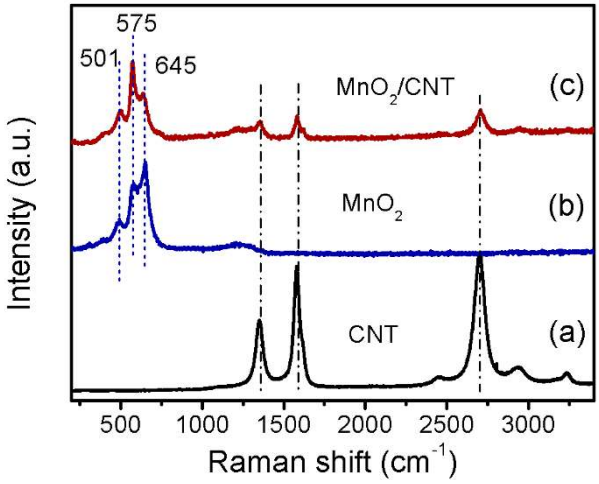

Figure 2 Raman spectra of the (a) pristine CNTs, (b) pure MnO_2, and (c) MnO_2/CNT nanocomposite.

Raman bands for the CNTs can be observed at the same time for the MnO_2/CNT nanocomposite. Therefore, the results of the Raman measurement agree well with the XRD results confirming that the birnessite-type MnO_2 has been formed during the hydrothermal treatment with or without the CNTs.

Morphologies of the CNTs, the birnessite-type MnO_2 powder, and the MnO_2/CNT nanocomposite are characterized by FESEM as shown in Figure 3. It can be observed in Figure 3a that the diameter of the CNTs is about 20 to 50 nm. In Figure 3b, it can be seen that the MnO_2 synthesized by hydrothermal reaction consists of monodisperse microspheres of 2 to 3 μm in diameter. The MnO_2 microspheres exhibit a flower structure composed of many nanoflakes radiating from the center. Figures 3c,d show the FESEM images of the MnO_2/CNT nanocomposite at low and high magnifications, respectively. It can be noted that the average diameter of the nanotubes increases for the MnO_2/CNT nanocomposite compared to the pristine CNTs, indicating that a thin MnO_2 layer has been coated on the CNT surface. The coated MnO_2 layer is uniform, exhibiting a highly porous structure.

TEM images of the MnO_2/CNT nanocomposite are shown in Figure 4. As shown in Figure 4a, the CNT core and the highly porous MnO_2 sheath resembling caterpillar-like morphology can be clearly seen. The K/Mn ratio obtained from EDX spectroscopy is about 0.2 as shown in the inset in Figure 4a. Figures 4b,c show the TEM images of a single CNT coated with porous MnO_2 at different magnifications. It can be seen that the porous MnO_2 layer is composed of numerous tiny nanoflakes, which are interconnected and uniformly distributed on the surface of the CNT. The interlayer

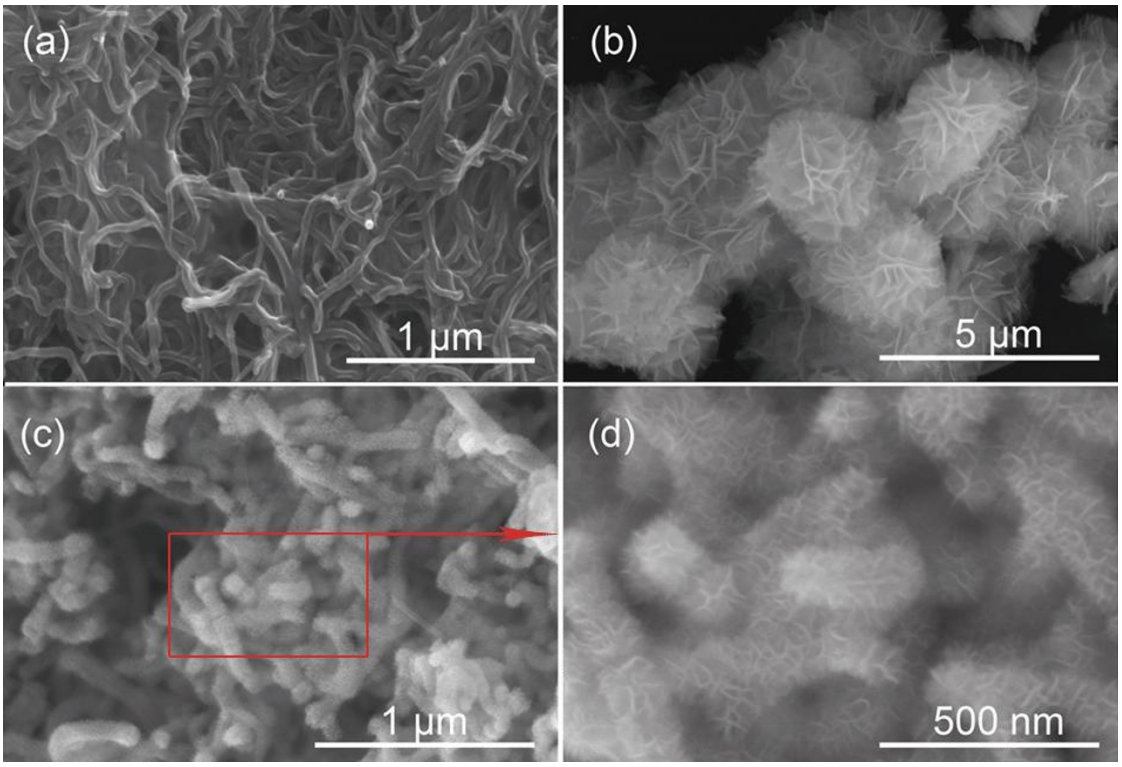

Figure 3 FESEM images. FESEM images of **(a)** the pristine CNTs, **(b)** the flower-like MnO_2 powder synthesized by hydrothermal reaction, and **(c)** the MnO_2/CNT nanocomposite synthesized by hydrothermal reaction. **(d)** A magnified FESEM image of the MnO_2/CNT nanocomposite synthesized by hydrothermal reaction.

water content and the CNT content can be evaluated from the TGA measurement as shown in the inset in Figure 4b. According to the weight loss of 6% below 250°C, the calculated interlayer water is around 0.33 H_2O per chemical formula ($K_{0.2}MnO_2{\cdot}0.33H_2O$). The weight loss of 28% at about 400°C is due to the oxidation of CNT in air [36]. Consequently, the composition of the MnO_2/CNT nanocomposite may be expressed as 72 wt.% ($K_{0.2}MnO_2{\cdot}0.33H_2O$)/28 wt.% CNT. For convenience, MnO_2/CNT is still used in the following text. The thickness of the porous MnO_2 layer is estimated to be about 20 nm as shown in Figure 4c. The inset in Figure 4c shows the electron diffraction [ED] pattern of the MnO_2 nanoflakes on the CNTs. Figure 4d shows the HRTEM image of the interface between the CNT and the MnO_2 layer. It can be seen that MnO_2 nanoflakes grow directly from the CNT walls, forming nearly vertically aligned MnO_2 nanoflake arrays. As shown in the inset in Figure 4e, the interplanar spacing of MnO_2 nanoflake has been measured to be 0.67 nm, which is in good agreement with approximately 0.7 nm as reported in the literature for birnessite-type MnO_2 [23,24]. Compared to the self-assembled MnO_2 nanoflakes of pure MnO_2 microspheres, these MnO_2 nanoflakes grown on CNTs are much smaller in dimension, typically with a thickness of less than 5 nm.

The formation mechanism of the present nanoarchitecture is discussed below. When the mixed solution with the CNT suspension and $KMnO_4$ is stirred at room temperature, a slow redox reaction between CNTs and $KMnO_4$ could take place and can be expressed as:

$$4MnO_4^- + 3C + H_2O \rightarrow 4MnO_2 + CO_3^{2-} + 2HCO_3^- . \quad (2)$$

The slow redox reaction usually leads to the precipitation of MnO_2 nanocrystallines on the surface of the CNTs. When the mixed solution is further undergone through the hydrothermal reaction, the redox reaction continues, but it may not be the major contribution to the later growth of MnO_2 nanoflakes on the CNTs. In the present experiments, stoichiometric amounts of $KMnO_4$ and CNTs were mixed in a solution based on Equation 2 for a hydrothermal reaction. After the hydrothermal reaction, no noticeable decrease in CNTs can be observed from the product, indicating that another reaction for the formation of MnO_2 may be dominant in the hydrothermal process. Porous MnO_2 films composed of nanoflakes have been reported to be easily

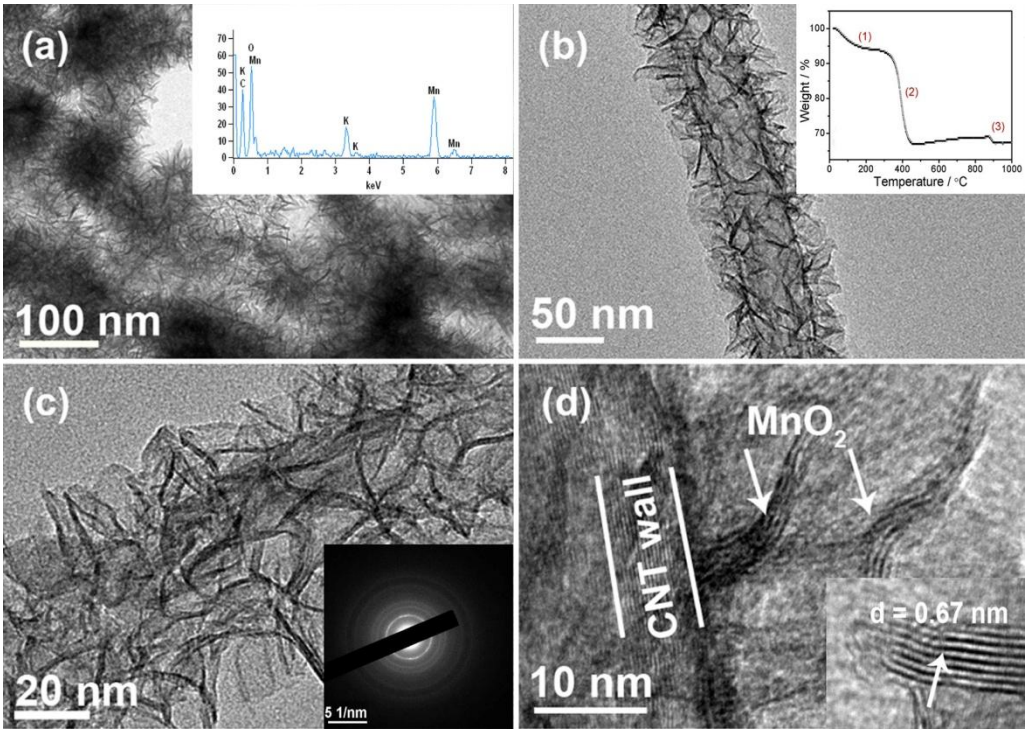

Figure 4 TEM and HRTEM images. **(a)** TEM image of the MnO_2/CNT nanocomposite. **(b)** TEM and **(c)** magnified TEM images of a single CNT coated with a porous MnO_2 layer. **(d)** HRTEM image of the interface between MnO_2 and CNT. Inset in (a) shows the EDX spectrum of the MnO_2/CNT nanocomposite. Inset in (b) shows the TGA spectrum of the MnO_2/CNT nanocomposite. Inset in (c) shows the ED pattern of the MnO_2/CNT nanocomposite. Inset in (d) shows the interplanar spacing of MnO_2 nanoflake grown on the CNT.

produced in a hydrothermal reaction of $KMnO_4$ solution without CNTs [24,25]. The formation of MnO_2 in such hydrothermal reaction is based on the decomposition of $KMnO_4$, which can be expressed as:

$$4MnO_4^- + 2H_2O \rightarrow 4MnO_2 + 4OH^- + 3O_2 \quad (3)$$

It is speculated that in the present solution system, the decomposition of $KMnO_4$ is much faster than the redox reaction between $KMnO_4$ and CNTs. During the hydrothermal reaction, the preformed MnO_2 nanocrystallines may serve as nucleation sites, where the newly formed MnO_2 nucleus due to the $KMnO_4$ decomposition could get deposited on. The flaky morphology is formed due to preferred growth along the ab plane of the layered birnessite-type MnO_2 [23,24]. Consequently, the CNT core/porous MnO_2 sheath hierarchy architecture could be easily produced using this simple hydrothermal method.

The specific surface area and pore size distribution of the MnO_2/CNT nanocomposite were obtained from an analysis of the desorption branch of N_2 gas isotherms using the density function theory. As shown in Figure 5c, an isotherm is typical for a mesoporous material with a hysteresis loop at high partial pressures. According to Brunauer-Emmett-Teller [BET] analysis, a total specific surface area of 237.8 m^2/g is obtained for the MnO_2/CNT nanocomposite, which is much larger than that of the pure MnO_2 (42.1 m^2/g, see Figure 5a) and that of the pristine CNTs (95.7 m^2/g, see Figure 5b). The Barrett-Joyner-Halenda [BJH] pore size distribution (Figure 5d) indicates that the MnO_2/CNT nanocomposites exhibit developed mesopores ranging from 2 to 8 nm, which may mainly be attributed to the numerous gaps between the MnO_2 nanoflakes.

The hierarchy architecture and high specific surface area of the MnO_2/CNT nanocomposite make it promising for applications in catalysis and in energy storage. In the present study, the electrochemical performance of the MnO_2/CNT nanocomposite as an electrode material in supercapacitors was investigated. Capacitive behaviors of the pristine CNT, the pure MnO_2, and the MnO_2/CNT nanocomposite electrodes in a 1-M Na_2SO_4 electrolyte at different scan rates are shown in Figure 6. The CV curves of the CNT electrode at different scan rates from 10 to 100 mV/s as shown in Figure 6a exhibit a rectangular shape without obvious redox peaks, indicating an ideal capacitive behavior. However, the specific capacitance of the pure CNT electrode is less than 25 F/

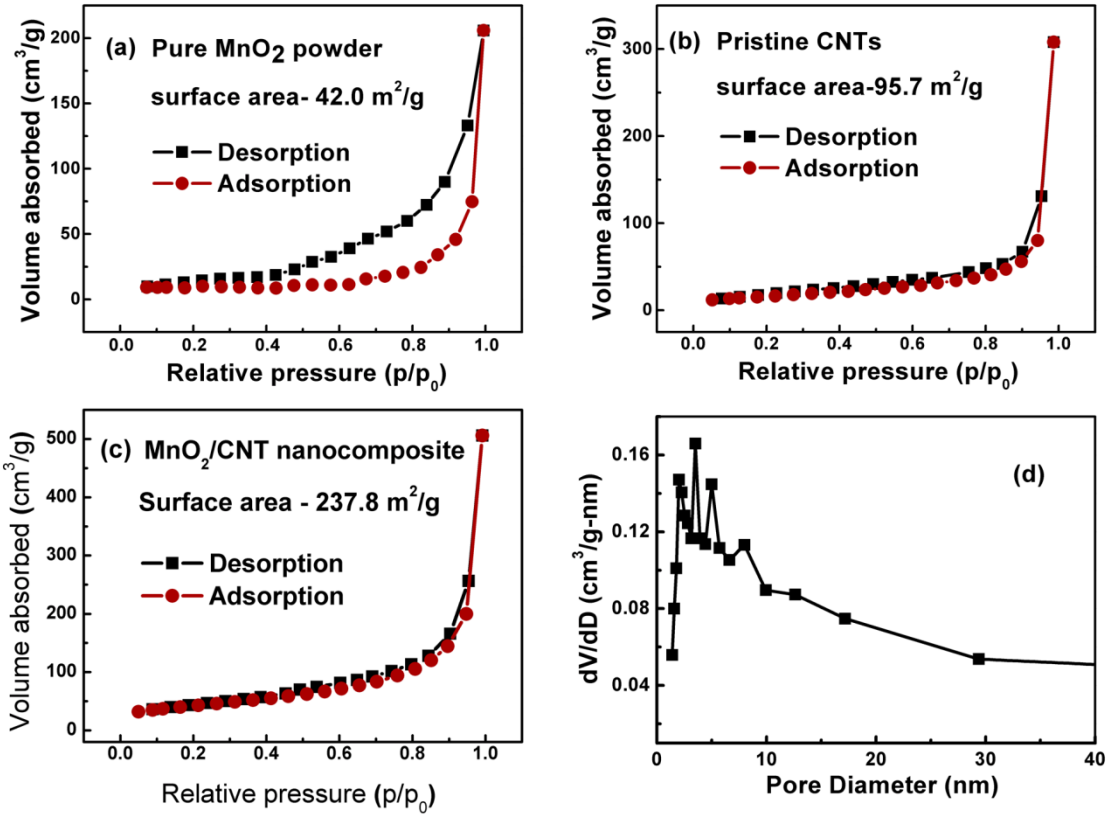

Figure 5 Nitrogen adsorption-desorption isotherms and BJH pore-size distributions. Nitrogen adsorption-desorption isotherms of **(a)** the pristine CNTs, **(b)** the MnO_2 powder, and **(c)** the MnO_2/CNT nanocomposite. **(d)** BJH pore-size distributions of the MnO_2/CNT nanocomposite.

g. Figure 6b shows the CV curves of the pure MnO_2 electrode at different scan rates. The current densities of the CV curves for the pure MnO_2 electrode increase significantly compared to those for the pure CNT electrode, which indicates that the MnO_2 electrode can deliver much higher capacitance. However, the rectangularity of the CV curves is significantly distorted as the scan rate increases, especially at a high scan rate of 100 mV/s. The specific capacitance of the MnO_2 electrode is about 123 F/g at a scan rate of 10 mV/s, while it decreases to 68 F/g at a scan rate of 100 mV/s. Figure 6c shows the CV curves of the MnO_2/CNT nanocomposite electrode at different scan rates. The current densities of the CV curves for the MnO_2/CNT nanocomposite electrode are even larger than those for the pure MnO_2 electrode, indicating higher specific capacitance and higher utilization of MnO_2 in the MnO_2/CNT nanocomposite electrode. The specific capacitance of the MnO_2/CNT nanocomposite electrode is about 223 F/g at a scan rate of 10 mV/s, corresponding to a high specific capacitance of 310 F/g for MnO_2 alone. CV curves of the MnO_2/CNT electrode maintain the rectangular shape even at a high scan rate of 100 mV/s with a high specific capacitance of 188 F/g. This is a significantly improved rate capability compared to that for the pure MnO_2 electrode. Figure 6d compares the specific capacitances at different scan rates for the three types of electrode materials. Although the CNT electrode has a very good rate capability, its specific capacitance is very low due to its surface adsorption charge storage mechanism for double layer capacitors. The pure MnO_2 electrode exhibits much larger specific capacitance compared with the CNT electrode due to the pseudocapacitance based on faradic redox reactions. However, the rate capability of the pure MnO_2 electrode is very poor, probably due to its intrinsically poor electronic conductivity and low specific surface area. By combining MnO_2 and CNT, the MnO_2/CNT nanocomposite exhibits the two advantages of the two electrode materials, namely a good rate capability and high specific capacitance. Several research groups have also reported the supercapacitive performance of the MnO_2/CNT nanocomposite [35-38]. Jin et al. [35] reported a MnO_2/CNT nanocomposite electrode with 65 wt.% MnO_2 delivering a specific capacitance of 144 F/g at a scan rate of 20 mV/s. The MnO_2/CNT nanocomposite

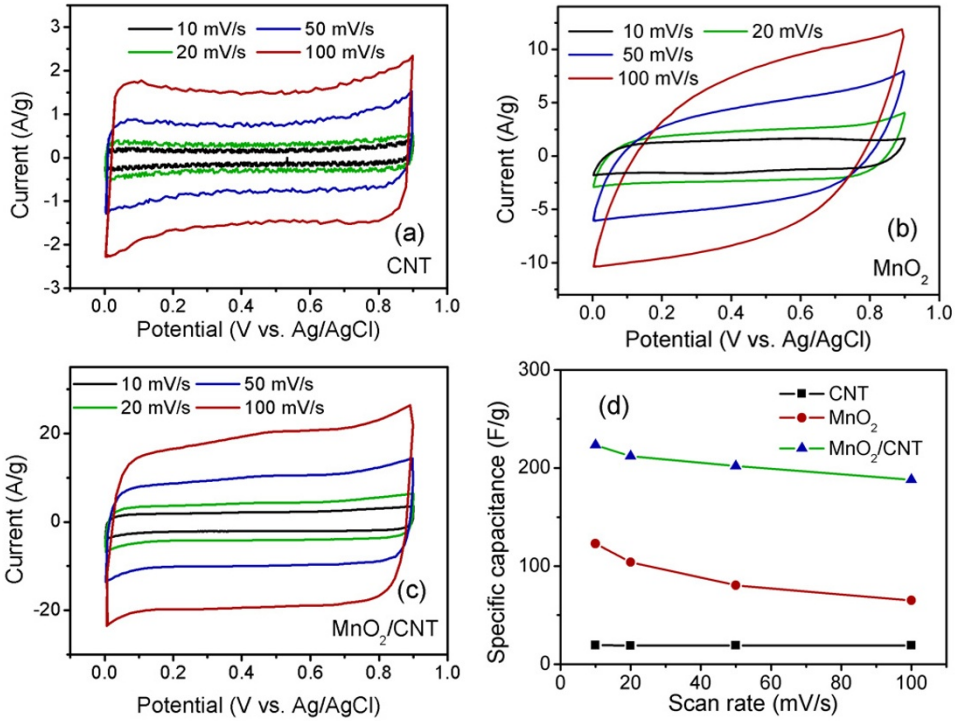

Figure 6 Cyclic voltammograms and specific capacitance vs. scan rate of the different electrodes. Cyclic voltammograms for the **(a)** CNT, **(b)** pure MnO_2, and **(c)** MnO_2/CNT nanocomposite electrodes in a 1-M Na_2SO_4 solution at different scan rates from 10 to 100 mV/s. **(d)** Specific capacitance vs. scan rate of the different electrodes.

electrode prepared by Xie et al. [36] was able to deliver a specific capacitance of 205 F/g at a scan rate of 2 mV/s, but only 43.2 F/g at a scan rate of 50 mV/s in a Na_2SO_4 electrolyte. The MnO_2/CNT nanocomposite electrode with 15 wt.% MnO_2 reported by Yan et al. [38] delivered a specific capacitance of 944 F/g at a scan rate of 1 mV/s based on the mass of MnO_2 alone or 141 F/g based on the total mass of the composite. From works reported in the literature so far, it appears difficult to achieve a specific capacitance above 200 F/g for the MnO_2/CNT composite in a Na_2SO_4 electrolyte. A high utilization of MnO_2 can only be achieved with a low mass ratio of MnO_2 in the composite, which, however, leads to a low specific capacitance of the composite. By increasing the mass ratio of MnO_2 in the composite with a thicker MnO_2 layer, the utilization of MnO_2 is reduced as only the surface area can be used for charge storage. The MnO_2/CNT nanocomposite electrode in the present study exhibits a superior supercapacitive performance with improved specific capacitance and rate capability compared to MnO_2/CNT nanocomposites in previous studies. The major difference between the MnO_2/CNT nanocomposite in the present study and those in previous works is the nanostructure of the MnO_2 layer. A highly porous MnO_2 layer composed of interconnected nanoflakes is introduced in the present study instead of a dense MnO_2 layer composed of closely packed nanocrystallines in previous works. The superior capacitive behavior of the present MnO_2/CNT nanocomposite electrode may be explained by its unique nanoarchitecture. Firstly, each MnO_2 nanoflake grows directly on the CNT surface. The CNTs construct a 3-D highly conductive current collector which significantly increases the electronic conductivity of the nanocomposite. Secondly, the large specific surface area and the nanoscopic MnO_2 phase of the MnO_2/CNT nanocomposite minimize the solid-state transport distances for both ions and electrons into MnO_2. This ensures a high utilization of the electrode materials, a high specific capacitance, and a good rate capability. Thirdly, the highly porous structure of the MnO_2 layer is able to minimize the diffusion distance of the electrolyte to the interior surfaces of MnO_2, which facilitates better penetration of the electrolyte into the electrode material and enhances the ionic conductivity of the electrode material. With this porous nanostructure of the MnO_2 layer, the utilization of MnO_2 can still be high even when the layer becomes thicker. This unique architecture enables the MnO_2/CNT nanocomposite electrode to have not only a large specific surface, but also a fast electron and ion transport, thus presenting the best electrochemical capacitive performance.

EIS measurements on the CNT, the pure MnO_2, and the MnO_2/CNT nanocomposite electrodes were performed at 0 V vs. Ag/AgCl, and the resulting Nyquist plots are displayed in Figure 7a. The Nyquist plots consist of (1) a high-frequency intercept on the real Z' axis, (2) a semicircle in the high-to-medium-frequency region, and (3) a straight line at the very low-frequency region. The high-frequency intercepts for all the three electrodes are almost the same, indicating that the three electrodes have the same combination resistance of ionic resistance of the electrolyte, intrinsic resistance of the active materials, and contact resistance between the active material and the current collector [41]. The semicircle in the high-to-medium-frequency region corresponds to a parallel combination of charge-transfer resistance (R_{ct}) and double-layer capacitance [42]. It can be seen that the R_{ct}, which is equal to the diameter of the semicircle, for the three electrodes is in the order of CNT < MnO_2/CNT < MnO_2. The R_{ct} of the MnO_2/CNT nanocomposite electrode is slightly larger than that of the CNT electrode, but much smaller than that of the pure MnO_2 electrode. It is speculated that the low R_{ct} of the MnO_2/CNT nanocomposite electrode is due to its high specific surface area, which facilitates a faster cation insertion/extraction process into/from the MnO_2 lattice. For a simple electrode-electrolyte system, the low-frequency straight line should exhibit a slope of 45° if the process is under diffusion control, or a slope of 90° if the system is purely capacitive in nature [43]. The almost vertical line for the CNT electrode here demonstrates a good capacitive behavior without diffusion limitation. The finite slope of the straight line represents the diffusive resistance of electrolyte in the electrode pores and cation diffusion in the host materials [41]. It can be seen that the slope of the straight line for the MnO_2/CNT nanocomposite electrode is similar to that of the CNT electrode, but much larger than that of the pure MnO_2 electrode. This observation suggests that the MnO_2/CNT nancomposite electrode has much lower diffusive resistance compared with the pure MnO_2 electrode. It is believed that the highly porous MnO_2 layer decorated on the surface of CNT is able to facilitate the penetration of the electrolyte, leading to fast diffusion of the electrolyte into the pores of the MnO_2 layer. For the pure MnO_2 electrode, although the microspheres of the self-assembled MnO_2 nanoflakes exhibit an open structure at the surface, the center area is quite dense. The latter buffers the electrolyte being diffused into the center area of the sphere. In addition, the dimension of the MnO_2 nanoflakes for the pure MnO_2 electrode is much larger compared with that of the MnO_2/CNT nanocomposite electrode so that the increased diffusion distances for both electrons and ions would also increase the diffusive resistance.

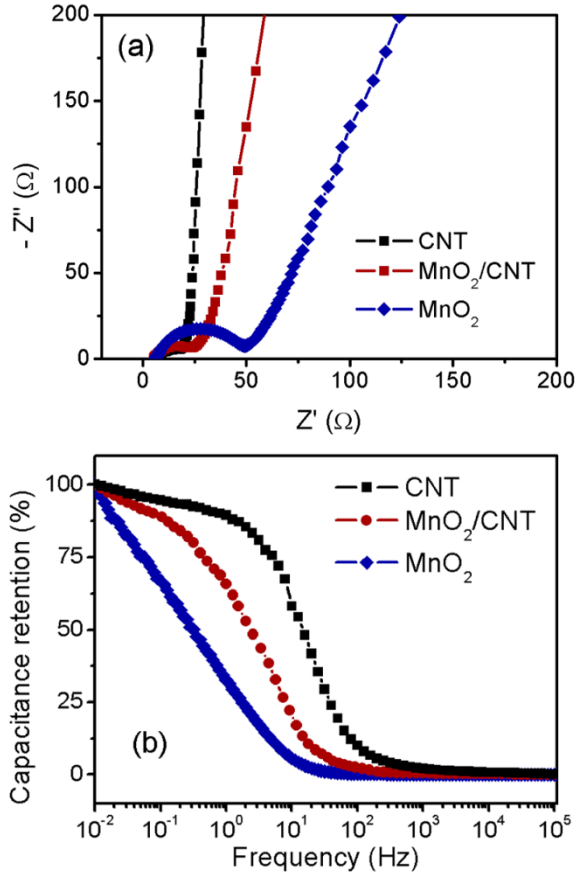

Figure 7 Nyquist plots and frequency dependence of capacitance retention of the electrodoes. **(a)** Nyquist plots and **(b)** frequency dependence of capacitance retention of the CNT, pure MnO_2, and MnO_2/CNT nanocomposite electrodes.

Figure 7b shows the capacitance retention as a function of frequency obtained by taking the real part of the complex capacitance $C^*(f) = 1/[i2\pi fZ^*(f)]$,where i, f, and Z^* are the imaginary unit, ac frequency, and complex impedance at a frequency, respectively [30,41,44]. For the porous electrode, the frequency response of capacitance may be understood using the parameter 'penetration depth,' $l' = 1/(fR'\ C')^{1/2}$, where R' and C' represent the pore resistance and pore capacitance per unit pore length, respectively [44]. At low frequency, when the electrolyte penetration depth is larger than the pore length of the porous electrode, most of the pore surface is utilized, resulting in a maximum capacitance. On the contrary, at high frequency, when the penetration depth is smaller than the pore length, only limited electrode surface is utilized, resulting in a decreased capacitance. As shown in Figure 7b, the capacitance retention for all three electrodes reaches the maximum at very low frequency, starts to decrease as the frequency increases,

and finally, goes down to zero at very high frequency. The CNT electrode exhibits an excellent rate capability with capacitance retention of 90% at a frequency of 1 Hz. The pure MnO_2 electrode however exhibits a poor rate capability with capacitance retention of only 32% at 1 Hz. It can be seen that a significantly improved rate capability can be obtained by combining the MnO_2 nanoporous sheath with the CNT core. The MnO_2/CNT nanocomposite is able to retain 65% of its full capacitance at 1 Hz. The significantly improved rate capability of the MnO_2/CNT nanocomposite electrode could be due to its small charge-transfer resistance and small diffusive resistance, indicating that the unique nanoarchitecture of CNT core/porous MnO_2 sheath is able to provide fast transport for both ions and electrons.

Conclusions

MnO_2/CNT nanocomposites with a unique nanoarchitecture consisting of a CNT core/porous MnO_2 sheath have been successfully synthesized using a simple hydrothermal treatment. The nanoporous MnO_2 sheath is composed of interconnected MnO_2 nanoflakes directly grown from the surface of the CNTs. The birnessite-type MnO_2 synthesized by the hydrothermal reaction contains 0.2 K^+ and 0.3 H_2O per formula. The nanoflaky MnO_2/CNT nanocomposite containing 72 wt.% MnO_2 exhibits a high specific surface area of 237 m^2/g with a pore distribution of 2 to 8 nm. The MnO_2/CNT nanocomposite electrode exhibits much higher specific capacitance compared with those of the CNT and the pure MnO_2 electrodes and a significantly improved rate capability compared to that of the pure MnO_2 electrode. The high specific capacitance of the MnO_2/CNT nanocomposite electrode may be attributed to the highly porous structure of the MnO_2 layer and its high specific surface area, resulting in high utilization of MnO_2. The significantly improved rate capability of the MnO_2/CNT nanocomposite electrode compared to that of the pure MnO_2 electrode could be explained by its small charge-transfer resistance and diffusive resistance obtained from EIS measurements, resulting from its unique hierarchy architecture where the 3-D electron path network constructed by the CNT cores and the nanoporous sheath composed of tiny MnO_2 nanoflakes facilitate faster electron and ion transport.

Acknowledgements

This research is supported by the National University of Singapore and the Agency for Science, Technology and Research through a research grant R-284-000-067-597 (072 133 0044). HX would like to thank Nanjing University of Science and Technology for the financial support through NUST Research Funding research grant (AB41385 and 2011ZDJH21).

Author details

[1]School of Materials Science and Engineering, Nanjing University of Science and Technology, 200 Xiao Ling Wei, Nanjing, 210094, China [2]Institute of Chemical and Engineering Science (ICES), 1 Pesek Road, Jurong Island, 627833, Singapore [3]Department of Mechanical Engineering, National University of Singapore, 9 Engineering Drive 1, 117576, Singapore

Authors' contributions

HX synthesized the MnO_2/CNT nanocomposite and performed the structural and electrochemical characterizations. YW and JYL carried out the BET experiments. LL conceived the study and revised the manuscript. All authors read and approved the final manuscript.

Competing interests

The authors declare that they have no competing interests.

Received: 5 September 2011 Accepted: 5 January 2012
Published: 5 January 2012

References

1. Li WN, Yuan JK, Gomez-Mower S, Xu LP, Sithambaram S, Aindow M, Suib SL: **Hydrothermal synthesis of structure- and shape-controlled manganese oxide octahedral molecular sieve nanomaterials.** *Adv Funct Mater* 2006, **16**:1247-1253.
2. Yan JA, Khoo E, Sumboja A, Lee PS: **Facile coating of manganese oxide on tin oxide nanowires with high-performance capacitive behavior.** *ACS Nano* 2010, **4**:4247-4255.
3. El-Deab MS, Ohsaka T: **Manganese oxide nanoparticles electrodeposite on platinum are superior to platinum for oxygen reduction.** *Angew Chem Int Ed* 2006, **45**:5963-5966.
4. Liu DW, Zhang QF, Xiao P, Garcia BB, Guo Q, Champion R, Cao GZ: **Hydrous manganese dioxide nanowall arrays growth and their Li^+ ions intercalation electrochemical properties.** *Chem Mater* 2008, **20**:1376-1380.
5. Wang LZ, Sakai N, Ebina Y, Takada K, Sasaki T: **Inorganic multilayer films of manganese oxide nanosheets and aluminum polyoxocations: fabrication, structure, and electrochemical behavior.** *Chem Mater* 2005, **17**:1352-1357.
6. Fei JB, Cui Y, Yan XH, Qi W, Yang Y, Wang KW, He Q, Li JB: **Controlled preparation of MnO_2 hierarchical hollow nanostructures and their application in water treatment.** *Adv Mater* 2008, **20**:452.
7. Wang X, Li YD: **Selected-control hydrothermal synthesis of alpha- and beta-MnO_2 single crystal.** *J Am Chem Soc* 2002, **124**:2880-2881.
8. Li ZQ, Ding Y, Xiong YJ, Yang Q, Xie Y: **One-step solution-based catalytic route to fabricate novel alpha-MnO_2 hierarchical structures on a large scale.** *Chem Commun* 2005, **7**:918-920.
9. Reddy ALM, Shaijumon MM, Gowda SR, Ajayan M: **Coaxial MnO_2/carbon nanotube array electrodes for high-performance lithium batteries.** *Nano Lett* 2009, **9**:1002-1006.
10. Simon P, Gogotsi Y: **Materials for electrochemical capacitors.** *Nat Mater* 2008, **7**:845-854.
11. Hu CC, Hung CY, Chang KH, Yang YL: **A hierarchical nanostructure consisting of amorphous MnO_2, $Mn3O_4$ nanocrystallites, and single-crystalline MnOOH nanowires for supercapacitors.** *J Power Sources* 2011, **196**:847-850.
12. Li GR, Feng ZP, Ou YN, Wu DC, Fu RW, Tong YX: **Mesoporous MnO_2/carbon aerogel composites as promising electrode materials for highperformance supercapacitors.** *Langmuir* 2010, **26**:2209-2213.
13. Chen S, Zhu JW, Han QF, Zheng ZJ, Yang Y, Wang X: **Shape-controlled synthesis of one-dimensional MnO_2 via a facile quick-precipitation procedure and its electrochemical properties.** *Cryst Growth Des* 2009, **9**:4356-4361.
14. Yu CC, Zhang LX, Shi JL, Zhao JJ, Cao JH, Yan DS: **A simple template-free strategy to synthesize nanoporous manganese and nickel oxides with narrow pore size distribution, and their electrochemical properties.** *Adv Funct Mater* 2008, **18**:1544-1554.
15. Hou Y, Cheng YW, Hobson T, Liu J: **Design and synthesis of hierarchical MnO_2 nanospheres/carbon nanotubes/conducting polymer ternary composite for high performance electrochemical electrodes.** *Nano Lett* 2010, **10**:2727-2733.

16. Xia H, Feng JK, Wang HL, Lai MO, Lu L: **MnO_2 nanotube and nanowire arrays by electrochemical deposition for supercapacitors.** *J Power Sources* 2010, **195**:4410-4413.
17. Xu CL, Zhao YQ, Yang GW, Li FS, Li HL: **Mesoporous nanowire array architecture of manganese dioxide for electrochemical capacitor applications.** *Chem Commun* 2009, **48**:7575-7577.
18. Ma RZ, Bando YS, Zhang LQ, Sasaki T: **Layered MnO_2 nanobelts: hydrothermal synthesis and electrochemical measurement.** *Adv Mater* 2004, **16**:918-922.
19. Kim IY, Ha HW, Kim TW, Paik YK, Choy JH, Hwang SJ: **Origin of improved electrochemical activity of beta-MnO_2 nanorods: effect of the Mn valence in the precursor on the crystal structure and electrode activity of manganates.** *J Phys Chem C* 2009, **113**:21274-21282.
20. Yang ZH, Zhang YC, Zhang WX, Wang X, Qian YT, Wen XG, Yang SH: **Nanorods of manganese oxides: synthesis, characterization and catalytic application.** *J Solid State Chem* 2006, **179**:679-684.
21. Zhang WX, Yang ZH, Wang X, Zhang YC, Wen XG, Yang SH: **Large-scale synthesis of beta-MnO_2 nanorods and their rapid and efficient catalytic oxidation of methylene blue dye.** *Catal Commun* 2006, **7**:408-412.
22. Zhang WX, Wang H, Yang ZH, Wang F: **Promotion of H_2O_2 decomposition activity over beta-MnO_2 nanorod catalysts.** *Colloids Surf A* 2007, **304**:60-66.
23. Liu ZP, Ma RZ, Ebina Y, Takada K, Sasaki T: **Synthesis and delamination of layered manganese oxide nanobelts.** *Chem Mater* 2007, **19**:6504-6512.
24. Zhu HT, Luo J, Yang HX, Liang JK, Rao GH, Li JB, Du ZM: **Birnessite-type MnO_2 nanowalls and their magnetic properties.** *J Phys Chem C* 2008, **112**:17089-17094.
25. Yan D, Yan PX, Cheng S, Chen JT, Zhuo RF, Feng JJ, Zhang GA: **Fabrication, in-depth characterization, and formation mechanism of crystalline porous birnessite MnO_2 film with amorphous bottom layers by hydrothermal method.** *Cryst Growth Des* 2009, **9**:218-222.
26. Umek P, Gloter A, Pregelj M, Dominko R, Jagodic M, Jaglicic Z, Zimina A, Brzhezinskaya M, Potocnik A, Filipic C, Levstik A, Arcon D: **Synthesis of 3D hierarchical self-assembled microstructures formed from alpha-MnO_2 nanotubes and their conducting and magnetic properties.** *J Phys Chem C* 2009, **113**:14798-14803.
27. Ni JP, Lu WC, Zhang LM, Yue BH, Shang XF, Lv Y: **Low-temperature synthesis of monodisperse 3D manganese oxide nanoflowers and their pseudocapacitance properties.** *J Phys Chem C* 2009, **113**:54-60.
28. Wang HQ, Li ZS, Huang YG, Li QY, Wang XY: **A novel hybrid supercapacitor based on spherical activated carbon and spherical MnO_2 in a non-aqueous electrolyte.** *J Mater Chem* 2010, **20**:3883-3889.
29. Toupin M, Brousse T, Belanger D: **Charge storage mechanism of MnO_2 electrode used in aqueous electrochemical capacitor.** *Chem Mater* 2004, **16**:3184-3190.
30. Fischer AE, Pettigrew KA, Rolison DR, Stroud RM, Long JW: **Incorporation of homogeneous, nanoscale MnO_2 within ultraporous carbon structures via self-limiting electroless deposition: implications for electrochemical capacitors.** *Nano Lett* 2007, **7**:281-286.
31. Zhang H, Cao GP, Wang ZY, Yang YS, Shi ZJ, Gu ZN: **Growth of manganese oxide nanoflowers on vertically-aligned carbon nanotube arrays for high-rate electrochemical capacitive energy storage.** *Nano Lett* 2008, **8**:2664-2668.
32. Ko JM, Kim KM: **Electrochemical properties of MnO_2/activated carbon nanotube composite as an electrode material for supercapacitor.** *Mater Chem Phy* 2009, **114**:837-841.
33. Wang YH, Liu H, Sun XL, Zhitomirsky I: **Manganese dioxide-carbon nanotube nanocomposites for electrodes of electrochemical supercapacitors.** *Scripta Mater* 2009, **61**:1079-1082.
34. Raymundo-Pinero E, Khomenko K, Frackowiak E, Beguin F: **Performance of manganese oxide/CNTs composites as electrode materials for electrochemical capacitors.** *J Electrochem Soc* 2005, **152**:A229-A235.
35. Jin XB, Zhou WZ, Zhang SW, Chen GZ: **Nanoscale microelectrochemical cells on carbon nanotubes.** *Small* 2007, **3**:1513-1517.
36. Xie XF, Gao L: **Characterization of a manganese dioxide/carbon nanotube composite fabricated using an in situ coating method.** *Carbon* 2007, **45**:2365-2373.
37. Ma SB, Nam KW, Yoon WS, Yang XQ, Ahn KY, Oh KH, Kim KB: **A novel concept of hybrid capacitor based on manganese oxide materials.** *Electrochem Commun* 2007, **9**:2807-2811.
38. Yan J, Fan ZJ, Wei T, Cheng J, Shao B, Wang K, Song LP, Zhang ML: **Carbon nanotube/MnO_2 composites synthesized by microwave-assisted method for supercapacitors with high power and energy densities.** *J Power Sources* 2009, **194**:1202-1207.
39. Sun ZY, Liu ZM, Han BX, Wang Y, Du JM, Xie ZL, Han GJ: **Fabrication of ruthenium-carbon nanotube nanocomposites in supercritical water.** *Adv Mater* 2005, **17**:928.
40. Ogata A, Komaba S, Baddour-Hadjean R, Pereira-Ramos JP, Kumagai N: **Doping effects on structure and electrode performance of K-birnessite-type manganese dioxides for rechargeable lithium battery.** *Electrochim Acta* 2008, **53**:3084-3093.
41. Xu MW, Kong LB, Zhou WJ, Li HL: **Hydrothermal synthesis and pseudocapacitance properties of alpha-MnO_2 hollow spheres and hollow urchins.** *J Phy Chem C* 2007, **111**:19141-19147.
42. Wei WF, Cui XW, Chen WX, Ivey DG: **Phase-controlled synthesis of MnO_2 nanocrystals by anodic electrodeposition: implications for high-rate capability electrochemical supercapacitors.** *J Phy Chem C* 2008, **112**:15075-15083.
43. Devaraj S, Munichandraiah N: **Electrochemical supercapacitor studies of nanostructured alpha-MnO_2 synthesized by microemulsion method and the effect of annealing.** *J Electrochem Soc* 2007, **154**:A80-A88.
44. Luo JY, Xia YY: **Effect of pore structure on the electrochemical capacitive performance of MnO_2.** *J Electrochem Soc* 2007, **154**:A987-A992.

doi:10.1186/1556-276X-7-33
Cite this article as: Xia *et al.*: Hydrothermal synthesis of MnO_2/CNT nanocomposite with a CNT core/porous MnO_2 sheath hierarchy architecture for supercapacitors. *Nanoscale Research Letters* 2012 **7**:33.